Jansen, K., Stupperich, E., & Fuchs, G. (1982) *Arch. Microbiol. 132*, 355–364.
Jones, W. J., Nagle, D. P., & Whitman, W. B. (1987) *Microbiol. Rev. 51*, 135–177.
Kanodia, S., & Roberts, M. F. (1983) *Proc. Natl. Acad. Sci. U.S.A. 80*, 5217–5221.
Keltjens, J. T., & van der Drift, C. (1986) *FEMS Microbiol. Rev. 39*, 259–303.
Lowry, O. H., Passonneau, J. V., Hasselberger, F. X., & Schulz, D. W. (1964) *J. Biol. Chem. 239*, 18–25.
Michal, G. (1974) in *Methods of Enzymatic Analysis* (Bergmeyer, H. U., Ed.) pp 1433–1438, Verlag Chemie, Weinheim, and Academic Press, New York.
Miller, T. L., & Wolin, M. J. (1983) *J. Bacteriol. 153*, 1051–1055.
Robertson, D., Lesage, S., & Roberts, M. F. (1989) *Biochim. Biophys. Acta 992*, 320–326.
Rose, Z. (1968) *J. Biol. Chem. 243*, 4810–4820.
Rose, Z., & Liebowitz, J. (1970) *J. Biol. Chem. 245*, 3232–3241.
Rudnick, H., Hendrich, S., Pilatus, U., & Blotevogel, K.-H. (1990) *Arch. Microbiol. 154*, 584–588.
Seely, R. J., & Fahrney, D. A. (1983) *J. Biol. Chem. 258*, 10835–10838.
Seely, R. J., & Fahrney, D. A. (1984) *J. Bacteriol. 160*, 50–54.
Tolman, C. J., Kanodia, S., Daniels, L., & Roberts, M. F. (1986) *Biochim. Biophys. Acta 886*, 345–352.
Zeikus, J. G., & Wolfe, R. S. (1972) *J. Bacteriol. 109*, 707–713.

Characterization of the Multiple EPR Line Shapes of Iron–Semiquinones in Photosystem 2†

Jonathan H. A. Nugent,* David C. Doetschman,‡ and Dugald J. Maclachlan

Department of Biology, Darwin Building, University College London, Gower Street, London WC1E 6BT, United Kingdom

Received August 14, 1991; Revised Manuscript Received December 31, 1991

ABSTRACT: We have compared the temperature-dependence characteristics of the EPR signals of Qa and Qb iron–semiquinones from both purple bacterial and plant photosystems. The data obtained were analyzed and estimates of the splitting parameters of the non-heme Fe^{2+} spin sublevels obtained. The study confirms the similarities of the $g = 1.8$ Qa iron–semiquinone signal ($D/k = 15.6$ K, $E/k = 3.3$ K) formed in formate-treated plant photosystem 2 to the signal found in purple bacteria. However, the $g = 1.9$ Qa iron–semiquinone signal ($D/k = 7.1$ K, $E/k = \ll 1$ K), formed in photosystem 2 when bicarbonate remains bound, has a unique temperature behavior. A series of spectral features associated with the iron–semiquinone in bicarbonate-bound photosystem 2 appear as the temperature is lowered, and the analysis of these data requires that some of these features be assigned to the higher spin states. The results are discussed in terms of the requirement for bicarbonate to be a ligand of the non-heme iron.

Photosystem 2 (PS2)[1] is a membrane–protein complex in algae, cyanobacteria, and plants which catalyzes the light-induced transfer of electrons from water to plastoquinone. The reaction center core complex of polypeptides and cofactors shows homology with that of purple photosynthetic bacteria. The purple bacterial reaction center has been studied extensively both structurally, from analysis of X-ray data, and functionally, by many biochemical and biophysical techniques (Michel et al., 1986; Michel & Deisenhofer, 1988; Feher et al., 1989).

In purple bacteria, the quinone electron acceptors Qa and Qb have binding sites on the core reaction center polypeptides L and M. Similar binding sites have been proposed for Qa and Qb of PS2 on the polypeptides D1(Qb) and D2(Qa), which show homology to the L and M polypeptides (Michel & Deisenhofer, 1988). In both PS2 and purple bacteria, a non-heme iron atom is located between the two quinone binding sites. Neither quinone provides a ligand to the non-heme iron. The function of the non-heme iron appears to be either electrostatic, influencing the properties of the bound quinones, or to maintain the structural integrity of the reaction center core.

The semiquinones of Qa and Qb can be detected by electron paramagnetic resonance (EPR) spectrometry. The line shape and g value of the signal obtained is influenced by the nearby non-heme iron, and the resulting "iron–semiquinone" spectra of both Qa and Qb in purple bacteria have a first-derivative peak near $g = 1.8$. The interaction between the non-heme iron and the semiquinone has been studied and the line shape simulated (Butler et al., 1984; Dismukes et al., 1984). Spin sublevels of the high-spin Fe^{2+} are split by a combination of spin–orbit and ligand field interactions. There is an exchange interaction between the semiquinone and the Fe^{2+}, perturbing the semiquinone EPR spectrum. The nature of the pertur-

† This work was supported by the U.K. Science and Engineering Research Council.
* Address correspondence to this author.
‡ Permanent address: Department of Chemistry, State University of New York, Binghamton, New York 13902-6000.

[1] Abbreviations: TBTQ, 2,3,5-tribromo-6-methyl-1,4-benzoquinone (tribromotoluquinone); HEPES, 4-(2-hydroxyethyl)-1-piperazineethanesulfonic acid; MES, 2-(*N*-morpholino)ethanesulfonic acid; EPR, electron paramagnetic resonance; OP, 1,10-phenanthroline; PS2, photosystem 2.

0006-2960/92/0431-2935$03.00/0

bation depends on the spin sublevel which the Fe^{2+} populates and thus upon the temperature.

The EPR of PS2 is complex in that more than one line shape form of the Qa iron–semiquinone signal is observed. Initially a line shape similar to the "g = 1.8 signal" of purple bacteria was identified (Nugent et al., 1981; Rutherford & Mathis, 1983). Subsequently, two more signals were identified, one at g = 1.9 (Rutherford & Zimmerman, 1984) and one at g = 1.6 (McDermott et al., 1988; Nugent et al., 1988). The "g = 1.9 signal" was observed above pH 7 and when bicarbonate was bound to the PS2 reaction center. The g = 1.8 signal was observed at low pH and when bicarbonate was displaced by formate (Vermaas & Rutherford, 1984). The "g = 1.6 signal" of Qa was initially found exclusively in cyanobacterial PS2 (McDermott et al., 1988; Nugent et al., 1988) but has now been detected in higher plant PS2 (Hallahan et al., 1991) and has been shown (Corrie et al., 1991) to arise from the interaction between the two semiquinones, $Qa^{\bullet-}$–Fe^{2+}–$Qb^{\bullet-}$.

In the purple bacterial reaction center, the ligands to the non-heme iron are four histidines and a bidentate glutamate residue (Michel et al., 1986; Feher et al., 1989). No effects indicative of bicarbonate binding have been detected in purple bacterial reaction centers. It has been suggested that the bicarbonate in PS2 binds at or close to the non-heme iron, replacing one or both of the iron–glutamate bonds present in purple bacteria (Michel & Deisenhofer, 1988).

The g value and line shape differences which exist between the three different signals of the PS2 iron–semiquinone Qa have been interpreted in terms of the purple bacterial model (Butler et al., 1984; Dismukes et al., 1984). This model implies that changes in physical parameters, especially the exchange interaction J between the iron and quinone radical, will change the g value and line shape. However, no systematic attempt to compare the PS2 and bacterial iron–semiquinone signals has been made.

The EPR spectrum of Qb iron–semiquinone in PS2 has received less attention. Rutherford et al. (1984) have observed a signal at g = 1.9, while Nugent et al. have observed both a g = 1.8 and g = 1.9 signal, attributed to Qb iron–semiquinone (Nugent et al., 1989; Hubbard et al., 1989). In recent measurements, we have characterized the EPR signals from the native Qb, a Qb analogue tribromotoluquinone, TBTQ, and their interactions with the Qa iron–semiquinone (Hallahan et al., 1991; Corrie et al., 1991).

We report measurements of the temperature dependence of Qa and Qb iron–semiquinone signals from both PS2 and purple bacteria, using procedures which ensure that only a single form is present in each measurement. The temperature-dependence data have been analyzed with a simplified procedure to estimate the splitting parameters of the Fe^{2+} spin sublevels, which are determined by the Fe^{2+} ligation. The results are important in assessing the differences between PS2 and purple bacteria in the ligation of the iron. This information about the electronic and spatial structure around the cofactors is also important because the structure determines the degree of overlap of electron density between the cofactors, a major influence on the rate of electron transfer in the reaction center.

Materials and Methods

Sample Preparation. Chloroplast thylakoid membranes [12 mg of chlorophyll (Chl)/mL] and PS2 enriched membranes (6 mg of Chl/mL, termed "PS2 membranes") were prepared by the method of Ford and Evans (1983) from market spinach (*Spinacea oleracea*) or pea (*Pisum sativum*) var Feltham First. A Triton X-100 detergent/Chl ratio of 22.5:1 was used at an incubation concentration of 2 mg of Chl/mL. Samples were stored and used in 20 mM MES-NaOH, 5 mM $MgCl_2$, 15 mM NaCl, and 20% (v/v) glycerol, pH 6.3.

Rhodopseudomonas viridis chromatophores were prepared as in Clayton and Clayton (1978) and used at a reaction center concentration of 20 μM. Chemical reduction of Qa was achieved by addition of sodium dithionite (25 μL of 40 mg/mL) to a dark-adapted sample treated with 5 mM *o*-phenanthroline (OP). The sample was frozen to 77 K after 15 min under nitrogen in the dark.

PS2 from the cyanobacterium *Phormidium laminosum* (1 mg of Chl/mL) was prepared as in Nugent et al. (1988) and Corrie et al. (1991). It was resuspended in 10 mM HEPES, 10 mM $MgCl_2$, 5 mM disodium hydrogen phosphate, and 25% (v/v) glycerol, pH 7.5.

Duplicate 0.3-mL EPR samples were placed in 3-mm diameter EPR tubes and treated as given in the text. Dimethyl sulfoxide or ethanol was used as solvent for TBTQ (600 μM) (Oettmeier et al., 1987; Renger et al., 1989) and OP (5 mM). The solvent concentration was kept below 2% (v/v). Sodium formate was used at 100 mM.

To maximize Qb semiquinone levels (Hallahan et al., 1991; Corrie et al., 1991), PS2 samples were illuminated for 30 s at room temperature with a 650-W light source fitted with a 2.5-cm water heat filter. The samples were then dark adapted at 273 K for 30–45 min, frozen to 77 K, and stored at 77 K in darkness until spectra were taken.

Illumination of PS2 at 77 K to reduce Qa was performed using an unfiltered 650-W light source directed at the sample placed in liquid nitrogen in a silvered Dewar. Five minutes illumination under these conditions produced maximum photoreduction of Qa.

EPR Spectrometry. EPR spectrometry was performed at cryogenic temperatures using a JEOL RE1X spectrometer fitted with an Oxford Instruments liquid helium cryostat. Spectra were recorded and manipulated using a Dell microcomputer running ASYST software. Measurements on the temperature dependence (Curie behavior) between 4.2 and 40 K of the g = 2 EPR signal of the PS2 tyrosine radical Y_D^+ ($S = {}^1/_2$) were used to confirm that the temperature calibration (signal size vs $1/T$) was linear over the range used.

Characteristic line shapes were established by examining several sets of samples involving different PS2 preparations. Microwave power levels were used which ensured that power saturation did not occur even at 4.2 K. Signal intensities were assigned to 100% either at the temperature of maximum amplitude or at the lowest temperature of measurement (4.2 K). The intensity measurements were taken between specific g values as indicated in the text. Errors of measurement are estimated to increase with temperature but be below ±10% at 30 K.

Analysis of Temperature Dependence Data. The theoretical models of the iron–semiquinone are based on a high-spin Fe^{2+} atom interacting with the semiquinone. Fe^{2+} is a non-Kramers ion, is EPR silent as a general rule, and is detectable only through its interaction with other magnetic species, e.g., through faster relaxation times induced on radicals or through changes in spectral line shapes and g values induced upon other species. The S = 2 ground manifold of the Fe^{2+}, which is split into five sublevels by spin–orbit and ligand field interactions, are in turn each split into doublets through an interaction with the spin on the semiquinone. The model of Dismukes et al. (1984) for the iron–semiquinone in purple bacteria uses Fe^{2+} spin splitting parameters D/k = 10.1 K and E/k = 2.4 K and

an isotropic exchange interaction (J_0 = 0.12 K) with the inclusion of a dipolar term to explain the broadening of some spectral features. The simulated spectrum involved the three lowest lying doublets. Butler et al. (1984) proposed an alternative model with D/k = 7.6 K and E/k = 1.9 K in which the interaction between semiquinone and iron is antiferromagnetic with an anisotropic exchange interaction (J_x = −0.13 K, J_y = −0.58 K and J_z = −0.58 K), the isotropic part of which is J_0 = −0.43 K. The spectrum was simulated from the two lowest lying doublets separated by 3.2 K.

The models for the simulation of purple bacterial iron–semiquinone EPR spectra have the following features on which we base a simplified analysis of the temperature dependences observed in this work. Many of the EPR spectral features can be associated with (1) particular members of the split Fe^{2+} spin manifold and (2) particular principal axes of the Fe^{2+} spin manifold splitting interaction. The magnitudes of the major splittings of the Fe^{2+} spin manifold (ca. D) are more than an order of magnitude greater than either the iron–semiquinone interaction or the interaction of the semiquinone spin with the magnetic field at the X-band frequencies employed in this work. Even the minor splittings (ca. $2E$) are much greater. Therefore one can expect to obtain D values of estimated 10% accuracy and possibly meaningful estimates of E simply by using the standard energy level expressions for an otherwise noninteracting Fe^{2+} spin manifold, $E = 2D$, $\pm 2D[1 + 3(E/D)^2]^{1/2}$, and $-D[1 \pm (3E/D)]$ [see Table IIB in Butler et al. (1984)], in order to describe the temperature dependence of the relative intensities of the EPR spectra of semiquinone perturbed by Fe^{2+} in each spin state. Under these assumptions, the semiquinone EPR intensity within a proportionality constant for an Fe^{2+} spin level i is given by

$$I_i = (1/ZT) \exp(-E_i/kT) \quad (1)$$

where Z is the partition function, the sum over all of the exponentials $\exp(-E_i/kT)$, i = 1, 2, ..., 5, and E_i are the energy level expressions for the Fe^{2+} spin manifold. This approach is used to interpret temperature-dependence data in terms of the energies of the spin levels of the various coupled iron–semiquinone systems.

Results

To simplify analysis of temperature-dependence measurements, PS2 samples were prepared and treated so that only one type of iron–semiquinone spectrum was observed in a particular sample. The EPR line shapes of Qa and Qb iron–semiquinones discussed are shown in Figures 1–5. The temperature dependences of the various signals illustrated qualitatively in Figures 2–5 have been measured systematically and are shown in Figure 6.

The *R. viridis* Qa iron–semiquinone spectrum, shown in Figure 1a, has a first-derivative peak at g = 1.84 and a trough near g = 1.7, which have a similar temperature dependence, as illustrated in Figure 2. The spectrum is sharpened by the addition of OP (Butler et al., 1984). Figure 2 shows that, as the temperature decreases, a shoulder appears on the high field side of the g = 1.84 feature and the broad shoulder on the low-field side of the g = 1.84 feature decreases. Similar effects were observed in the broader g = 1.84 peak of PS2 treated with formate (Figures 1b and 3) with the low-field shoulder decreasing as the temperature was lowered. Figure 3 shows that in the formate-treated PS2 sample, the g = 1.7 trough moves to higher field (g = 1.72 to g = 1.69) as the temperature is lowered.

Figure 4 shows the spectrum of untreated (bicarbonate bound) PS2 Qa iron–semiquinone at two temperatures illus-

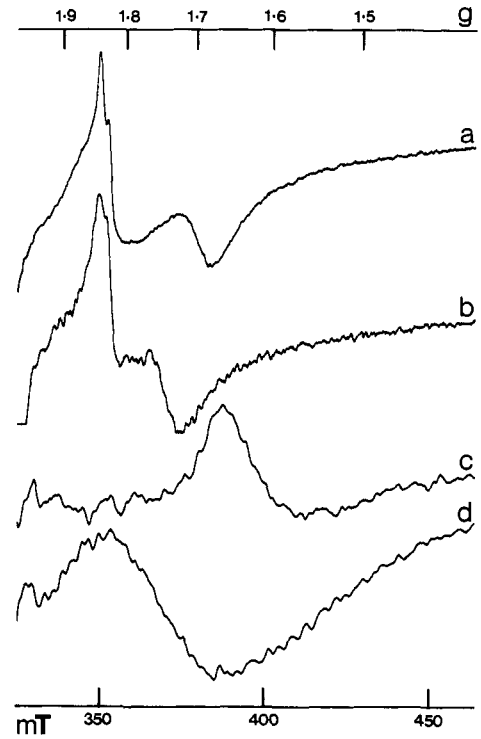

FIGURE 1: EPR spectra at 4.5 K showing some of the Qa and Qb iron–semiquinone line shapes investigated. (a) Qa iron–semiquinone of *R. viridis* chromatophores treated with *o*-phenanthroline. (b) Qa iron–semiquinone of pea PS2 membanes treated with formate. (c) Spectrum of *P. laminosum* PS2 showing the g = 1.66 signal from $Qa^{\bullet-}$–Fe^{2+}–$Qb^{\bullet-}$. (d) Qb iron–semiquinone of pea PS2 membranes treated with TBTQ. Iron–semiquinone in spectrum a was induced by chemical reduction and in spectra b–d by photochemical reduction as given under Materials and Methods. EPR conditions: microwave power, 5 mW; modulation width, 1.25 mT.

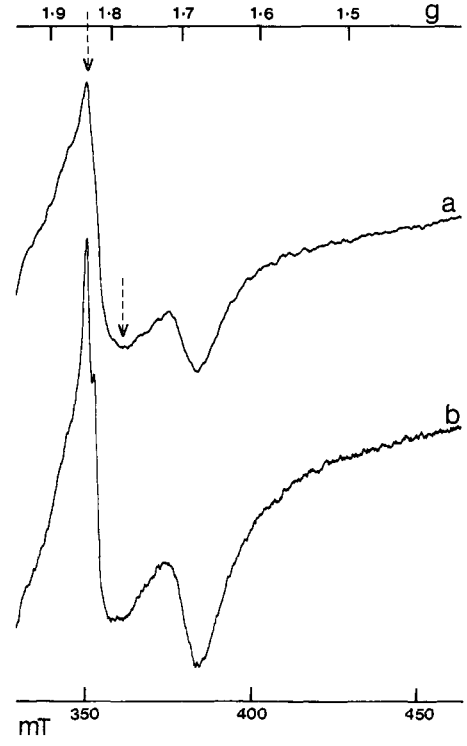

FIGURE 2: Illustration of the temperature dependence of the Qa iron–semiquinone line shape in *R. viridis* chromatophores treated with *o*-phenanthroline. EPR conditions: microwave power, 1 mW; modulation amplitude, 1.25 mT; temperature (a) 13 K and (b) 4.4 K; instrument gain: spectrum a = 3 × spectrum b. Other conditions are as given in the legend to Figure 1. Arrows indicate g values where measurements were made.

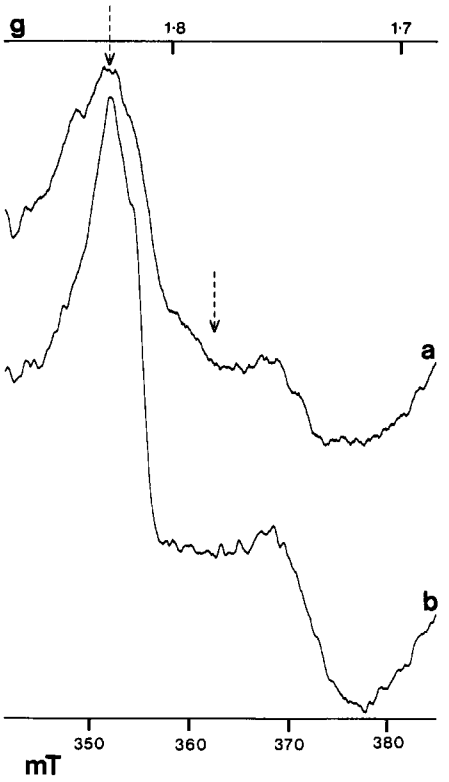

FIGURE 3: Illustration of the temperature dependence of the Qa iron–semiquinone line shape of spinach PS2 membranes treated with formate. (a) 15 K. (b) 4.3 K. Other conditions are as given in the legend to Figure 1. Arrows indicate g values where measurements were made.

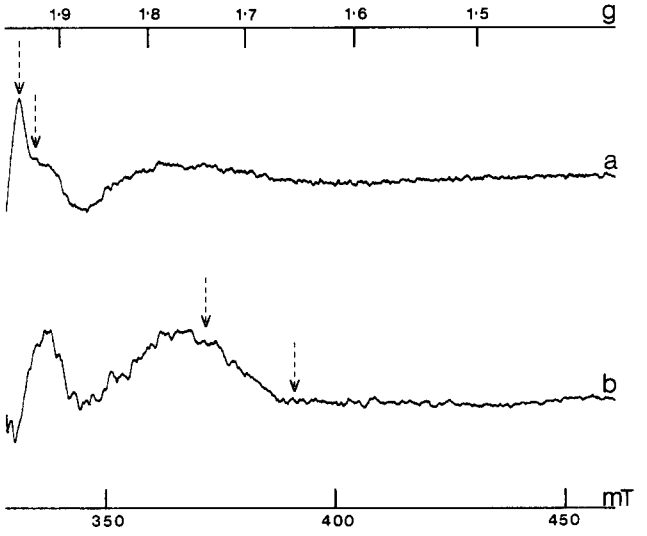

FIGURE 4: Illustration of the temperature dependence of the Qa iron–semiquinone line shape of pea PS2 membranes in its native (bicarbonate-bound) state. (a) 15 K. (b) 4.4 K. EPR conditions: microwave power, 2 mW; same instrument gain in both spectra. Other conditions are as given in the legend to Figure 1. Arrows indicate g values where measurements were made.

trating the line shape changes and the peaks near $g = 1.75$ and $g = 1.95$ used in the systematic temperature-dependence measurements. The additional feature near $g = 1.9$ shows a temperature dependence that is intermediate between the temperature dependences of the $g = 1.95$ and $g = 1.75$ peaks. The whole $g = 1.9$ feature broadens and moves to higher field as the temperature is lowered.

Figures 1d and 5a,b show PS2 samples containing the Qb analogue TBTQ, while Figure 5c,d shows the native Qb

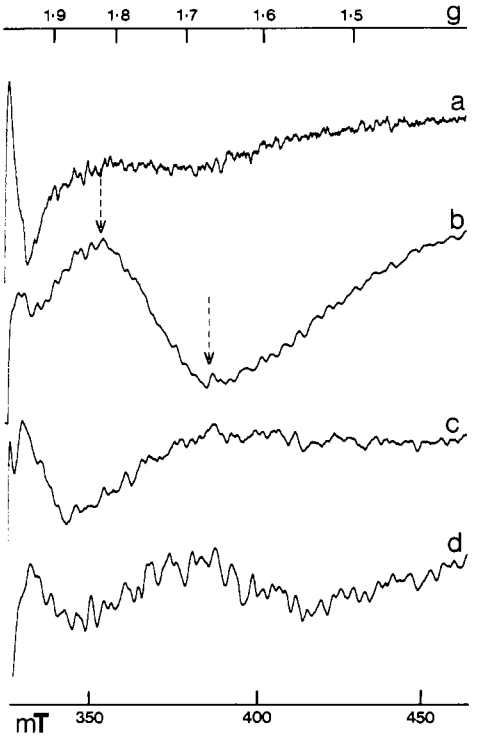

FIGURE 5: Illustration of the temperature dependence of the Qb iron–semiquinone line shape. (a) Pea PS2 membranes treated with TBTQ, recorded at 17 K; (b) with TBTQ, recorded at 4.3 K; (c) pea thylakloid membranes in a native (bicarbonate-bound) state at 15 K; (d) in a bicarbonate-bound state at 4.4 K. EPR conditions: microwave power, 5 mW; modulation amplitude, 1 mT. Other conditions are as given in the legend to Figure 1. Arrows indicate g values where measurements were made.

Table I: D and E Parameters of Iron–Semiquinones[a]

iron–semiquinone	D/k (K)	E/k (K)
Qa *R. viridis*	11.8 (1.2)	2.7 (0.7)
Qa PS2 plus formate	15.6 (0.3)	3.3 (0.9)
Qb PS2 plus TBTQ	24.7 (2.7)	0[b]
Qa PS2 (bicarbonate bound)	7.1 (0.4)	0[b]

[a] Results of the least-squares adjustment to the EPR intensity data for the indicated iron–semiquinones given in curves b–e in Figure 6. Figures given in parentheses are the standard deviations of the parameters from the fit. [b] E was assumed to be zero in these fits and was shown to be small relative to D in a fit where both were varied.

iron–semiquinone. Figure 5 illustrates that the untreated (bicarbonate bound) Qb iron–semiquinone has a temperature dependence that is qualitatively similar to the corresponding Qa 1.9 EPR signal. However, owing to the weak signal of the untreated Qb iron–semiquinone, the systematic measurements of the temperature dependence were carried out only for the artificial TBTQ Qb iron–semiquinone spectra. The EPR signals observed with TBTQ were of two types, a $g = 1.98$ peak (Figure 5a) characteristic of bicarbonate-bound $g = 1.9$ iron–semiquinone and a broad signal (Figure 5b) with a peak near $g = 1.8$, more characteristic of $g = 1.84$ iron–semiquinone where bicarbonate is replaced by formate.

The temperature-dependence characteristics of the iron–semiquinones are shown in Figure 6. Similar increases in signal size with decreasing temperature were obtained for the various signal forms except for the $g = 1.95$ peak in bicarbonate-bound PS2, which showed a pronounced maximum.

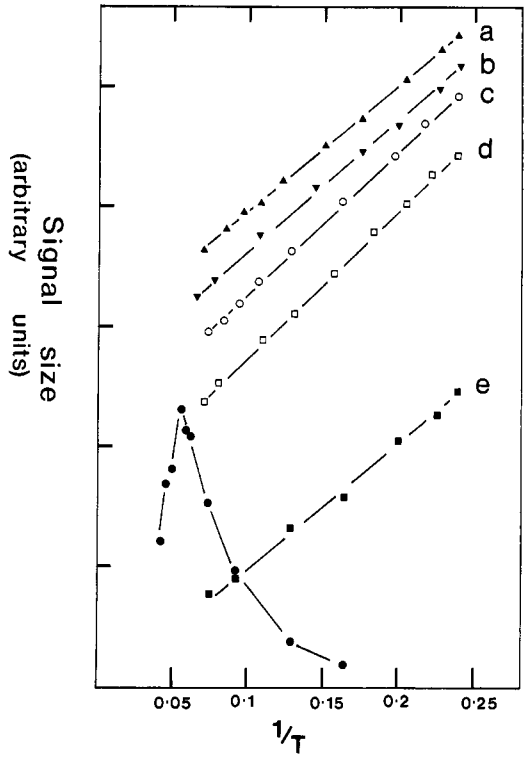

FIGURE 6: Temperature dependences (signal size vs $1/T$) of the various Qa and Qb iron–semiquinone EPR line shapes. (a) $Qa^{\bullet-}$–Fe^{2+}–$Qb^{\bullet-}$ in *P. laminosum* PS2, measured as the peak height at $g = 1.66$. (b) TBTQ Qb iron–semiquinone in pea PS2 membranes, measured between $g = 1.815$ and $g = 1.67$. (c) Qa iron–semiquinone of *R. viridis* treated with *o*-phenanthroline measured between $g = 1.84$ and $g = 1.79$. (d) Qa iron–semiquinone of pea PS2 membranes treated with formate measured between $g = 1.84$ and $g = 1.78$. (e) Qa iron–semiquinone of pea PS2 membranes in its native (bicarbonate-bound) state: (■) measured between $g = 1.73$ and $g = 1.65$; (●) measured between $g = 1.95$ and 1.925. Each set of measurements were normalized using the maximum signal size. The plots, all to the same scale, are displaced vertically for clarity. For further details see Materials and Methods. EPR conditions are as in Figures 2–5.

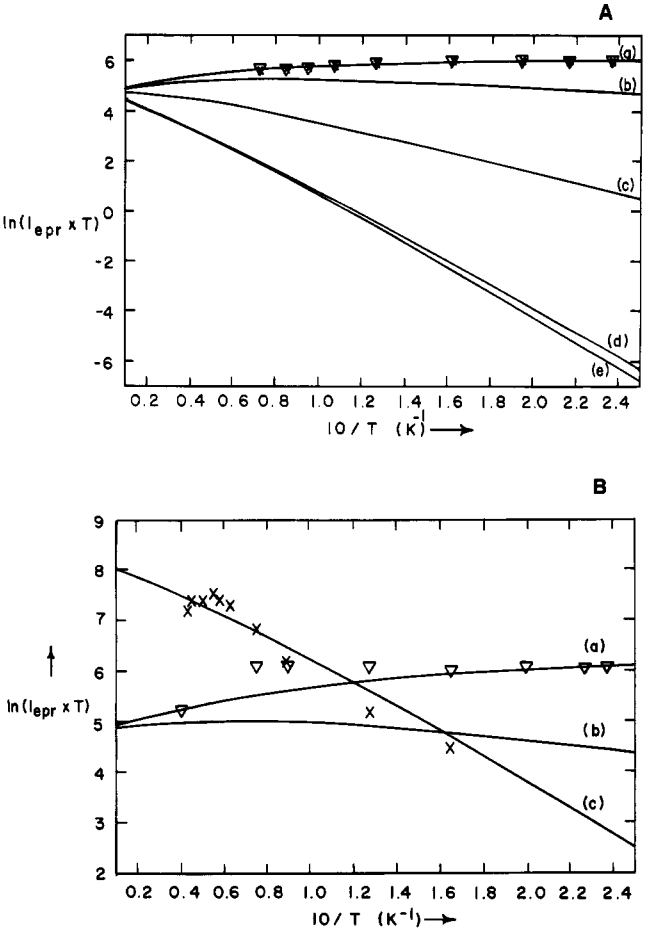

FIGURE 7: Calculated and experimental temperature dependence of the Qa iron–semiquinone EPR spectra of (A) *R. viridis* and (B) bicarbonate-bound pea PS2 membranes. The intensities were calculated with the best fit D and E values given in Table I with the energy expressions given in the text and the intensity expression given in eq 1. (A) Theoretical curves for (a) ground, (b) first, (c) second, (d) third, and (e) highest spin states of the $S = 2$ Fe^{2+} of *R. viridis*. The experimental relative intensities are represented by the (▽) $g = 1.7$ and (×) $g = 1.84$ features in the iron–semiquinone spectrum. (B) Theoretical curves for (a) ground, (b) first, and (c) highest spin states of pea PS2 membranes. The experimental relative intensities are represented by the $g = 1.73$ peak (▽) and the $g = 1.95$ peak (×).

The data shown in Figure 6 for the various iron-semiquinones were fitted with eq 1 by least-squares adjustment of the D and E parameters, and the results are presented in Table I. The EPR spectral features to which the single curves a–d correspond were assumed to be from interactions of the semiquinone with the lowest energy Fe^{2+} spin state ($i = 1$ in eq 1). Although this assumption has either been generally accepted or can be argued by analogy, it was also demonstrated directly that the data could not be fitted satisfactorily by assuming an interaction with an excited Fe^{2+} spin level ($i > 1$ in eq 1).

In the fits to the TBTQ Qb iron–semiquinone and bicarbonate-bound PS2 Qa iron–semiquinone data (curves b and e in Figure 6), a satisfactory fit to D was obtained only when E was assumed to be zero. When both D and E values were fit to the data, E was small relative to D, but their values were not meaningful in view of their large standard deviations.

The temperature dependence of the $g = 1.66$ signal from *P. laminosum* PS2 in Figure 1c and the absence of any line shape change upon warming supports the assignment of this peak to $Qa^{\bullet-}$–Fe^{2+}–$Qb^{\bullet-}$. A minimum could not be found for the fit to Figure 6 curve a for $Qa^{\bullet-}$–Fe^{2+}–$Qb^{\bullet-}$, but the curve could be acceptably reproduced with ratios of D and E values (not shown) which fell in the ranges of the other iron–semiquinone D and E values in Table I.

For the PS2 bicarbonate-bound Qa iron–semiquinone, the $g = 1.7$ (squares) curve e of Figure 6 was taken to be from an interaction with the ground-state Fe^{2+} (and could not be fit by assuming an excited-state interaction). From its general behavior, the $g = 1.95$ (circles) curve e was assumed to be from an interaction with one of the excited spin levels of the Fe^{2+}. Only the assumption that the feature arose from the highest ($i = 5$) excited state gave a satisfactory simultaneous fit of eq 1 ($i = 1, 5$) to the data shown in Figure 6, curve e.

Figure 7 illustrates how the experimental data for the *R. viridis* and bicarbonate-bound PS2 Qa iron–semiquinone EPR signals fit the calculated curves for the non-heme Fe^{2+} spin states. Figure 7A shows that the temperature dependences of the *R. viridis* iron–semiquinone feature at $g = 1.84$ and the trough at $g = 1.7$ are not very different, contrary to what would be expected if they were from the ground (a) and first excited (b) states. The best fit to these temperature dependences was obtained by assuming that both were from the ground state (with $E/k = 2.7$ K ± 0.7 K) rather than by assuming that they were from a mixture of ground and first excited state intensities. Figure 7B shows that the experimental data for the $g = 1.95$ peak of the bicarbonate-bound PS2 iron semiquinone fits the highest excited state (c). Only measurements up to 30 K are shown, as the fit was worse when using measurements at higher temperatures, reflecting the small signal size and the increased error on the temperature measurement

at >30 K. The $g = 1.73$ peak is shown fit to the ground state (a). The deviation at higher temperatures again reflects the small signal size and the overlap of features from higher states at >10 K.

Discussion

Our results give a reasonable agreement for the Fe^{2+} spin level splitting parameters for *R. viridis* Qa iron–semiquinone with those of Dismukes et al. (1984) and Butler et al. (1984), giving confidence in our analysis for the various PS2 iron–semiquinone signals.

The assignment for the first time of EPR features to an interaction with Fe^{2+} in its highest excited spin state as found in native bicarbonate-bound PS2 iron–semiquinones is interesting. Previous failures to observe features from interaction with the higher excited Fe^{2+} spin states have generally been attributed to fast spin relaxation. The unusually small Fe^{2+} spin level splitting parameter in the bicarbonate-bound PS2 may reduce the spin relaxation rates. The simulations of Butler et al. (1984) predict spectra for the semiquinone interacting with the Fe^{2+} in its fourth and fifth excited spin states that are similar to those with the ground and first excited states, with a narrow line near $g = 2$ predicted for interaction with the third excited state. These predictions for *R. viridis* appear to be in qualitative agreement with the observation of a ground-state feature at $g = 1.7$ and an intermediate temperature dependence above $g = 1.9$ from one of the excited states $i = 2$–4 in the bicarbonate-bound PS2 iron–semiquinone EPR spectra.

The behavior of purple bacterial Qa observed here is similar to that previously described in Butler et al. (1984) and Wraight (1978). Evelo et al. (1988) used EPR experiments on single crystals of *R. viridis* to assign the two features found near $g = 1.8$ as $1.81 = 2x$ and $1.83 = 1z$ (where the numbers indicate the x, y, and z axes of a particular doublet in ground and excited states), but no temperature measurements were reported to support this. The temperature data of Butler et al. (1984) and the data reported here show that the opposite is correct, $g = 1.81 = 1z$, i.e., the ground state, and that $g = 1.83 = 2x$. Evelo et al. (1988) also assumed that the trough near $g = 1.7$ originated from the $2z$ (first excited state) field position. The temperature dependence of both the *R. viridis* and formate-treated PS2 iron–semiquinone spectra measured at the $g = 1.7$ trough indicate that it cannot arise from the first excited state $2z$ alone. This is supported by the temperature-dependent g value shifts indicated in Figure 3. This feature probably arises from a superposition of $2z$ and $1x$, which are both broadened by a strong dependence on J_z and J_x, respectively (Butler et al., 1984).

There is considerable variation in the D splitting parameters for the Fe^{2+} in the various iron–semiquinones studied. This is consistent with the different ligation of the iron that is suggested by structural studies and homology considerations (Michel et al., 1986; Michel & Deisenhofer, 1988). There is a marked change when the bicarbonate bound in native PS2 is displaced by formate. The previously mentioned spectral similarity between the *R. viridis* and formate-bound PS2 EPR is reflected in similar splitting parameters, in E/k values that are equal within experimental error and D/k values that are nearest in order of size. This may result, for example, from the similarity in formate and glutamate carboxylate ligation to the iron or perhaps from glutamate ligation in PS2 in the absence of bicarbonate.

The markedly higher D value for the TBTQ is puzzling in that binding of TBTQ to the Qb site would not be expected to influence the Fe^{2+} ligand field. The possibility of a large TBTQ heavy atom effect on the Fe^{2+} spin would not appear to be likely in view of the weak coupling and long distance between iron and semiquinone. However, Qb in purple bacteria is hydrogen bonded to one of the iron liganding histidines (Sinning et al., 1989b) so that TBTQ binding in a similar position in PS2 may alter the way in which the iron ligand D1 histidine 215 binds to the non-heme iron.

A question yet to be answered in PS2 is whether bicarbonate directly ligates to the non-heme iron. We have recently shown that bicarbonate binding does cause the shift in g value to $g = 1.9$ (Bowden et al., 1991). A shift of the Qa and Qb iron–semiquinone peaks from $g = 1.8$ should involve structural changes in the first coordination sphere of the non-heme iron. It therefore follows that the shift of g value from 1.8 to 1.9 caused by bicarbonate binding must occur through an effect on the iron ligands. Previous PS2 experiments, including those from EPR and Mössbauer studies, have indicated that the bicarbonate binds to the non-heme iron (Nugent et al., 1988; Blubaugh & Govindjee, 1988; Diner & Petrouleas, 1990). However, two bicarbonate binding sites are required to explain all the data (Blubaugh & Govindjee, 1988).

EPR signals from Qb iron–semiquinone in the purple bacterium *Rhodospirillum rubrum* were found to have g value ($g = 1.93$), line shape, and temperature-dependence properties similar to those of $g = 1.9$ signals in PS2 (Beijer & Rutherford, 1987). No bicarbonate binding is observed in *R. rubrum*, and the amino acid sequence has only minor differences to that of other purple bacteria. Recently, a mutant of *R. viridis* has been isolated which has a Qb iron–semiquinone spectrum similar to that of *R. rubrum* and PS2 (Sinning et al., 1989a,b), whereas the Qa iron–semiquinone is normal. This mutant only has a single amino acid change in the Qb binding loop. These results imply that changes in the EPR characteristics of the iron–semiquinone in PS2 upon bicarbonate binding do not require that the bicarbonate binds directly to the non-heme iron. The EPR effects indicative of changes in the first coordination sphere may possibly be mediated through the histidine ligands, via alterations in the pK's of amino acid side chains due to the presence or absence of bicarbonate.

Analysis of the D1 and D2 amino acid sequences in the quinone binding regions reveals conserved positively charged sites one α-helical turn above the iron-liganding histidines D1 272 and D2 269. An approximately symmetrical binding of two bicarbonates, one at D2 lysine 265/arginine 266 and the other to arginine D1 269 would account for the experimental evidence. As bicarbonate is potentially a bidentate ligand, these sites may also provide one or two ligands to the non-heme iron. In any case, loss of bicarbonate from these sites would produce a change in the pK's of the histidine ligands affecting the EPR properties of the non-heme iron. This effect on the histidine ligands provides a possible mechanism for the EPR changes observed in both the purple bacterial and PS2 experiments.

Acknowledgments

We thank Professor W. Oettmeier for his gift of TBTQ, and we also thank Professor M. C. W. Evans, Dr. P. Heathcote, and Dr. S. Rigby for helpful discussions.

Registry No. Bicarbonate, 71-52-3.

References

Beijer, C., & Rutherford, A. W. (1987) *Biochim. Biophys. Acta 890*, 169–178.

Blubaugh, D. J., & Govindjee (1988) *Photosynth. Res. 19*, 85–128.

Bowden, S. J., Hallahan, B. J., Ruffle, S. V., Evans, M. C. W., & Nugent, J. H. A. (1991) *Biochim. Biophys. Acta 1060*, 89–96.
Butler, W. F., Calvo, R., Fredkin, D. R., Isaacson, R. A., Okamura, M. Y., & Feher, G. (1984) *Biophys. J. 45*, 947–973.
Clayton, B. J., & Clayton, R. K. (1978) *Biochim. Biophys. Acta 501*, 470–487.
Corrie, A. R., Nugent, J. H. A., & Evans, M. C. W. (1991) *Biochim. Biophys. Acta 1057*, 384–390.
Diner, B. A., & Petrouleas, V. (1990) *Biochim. Biophys. Acta 1015*, 141–149.
Dismukes, G. C., Frank, H. A., Friesner, R., & Sauer, K. (1984) *Biochim. Biophys. Acta 764*, 253–271.
Evelo, R. G., Nan, H. M., & Hoff, A. J. (1988) *FEBS Lett. 239*, 351–357.
Feher, G., Allen, J. P., Okamura, M. Y., & Rees, D. C. (1989) *Nature 339*, 111–116.
Ford, R. C., & Evans, M. C. W. (1983) *FEBS Lett. 160*, 159–164.
Hallahan, B. J., Ruffle, S. V., Bowden, S. J., & Nugent, J. H. A. (1991) *Biochim. Biophys. Acta 1059*, 181–188.
Hubbard, J. A. M., Corrie, A. R., Nugent, J. H. A., & Evans, M. C. W. (1989) *Biochim. Biophys. Acta 977*, 91–96.
McDermott, A. E., Yachandra, V. K., Guiles, R. D., Cole, J. L., Dexheimer, S. L., Britt, R. D., Sauer, K., & Klein, M. P. (1988) *Biochemistry 27*, 4021–4031.
Michel, H., & Deisenhofer, J. (1988) *Biochemistry 27*, 1–7.
Michel, H., Epp, O., & Deisenhofer, J. (1986) *EMBO J. 5*, 2445–2451.
Nugent, J. H. A., Diner, B. A., & Evans, M. C. W. (1981) *FEBS Lett. 124*, 241–244.
Nugent, J. H. A., Corrie, A. R., Demetriou, C., Evans, M. C. W., & Lockett, C. J. (1988) *FEBS Lett. 235*, 71–75.
Nugent, J. H. A., Corrie, A. R., Hubbard, J. A. M., Bowden, S. J., Demetriou, C., Lockett, C. J., & Evans, M. C. W. (1989) in *Photoconversion Processes for Energy and Chemicals* (Hall, D. O., & Grassi, G., Eds) pp 190–197, Elsevier Applied Science Publishers, London.
Renger, G., Messinger, J., & Fromme, R. (1989) *Z. Naturforsch. 44c*, 423–430.
Rutherford, A. W., & Mathis, P. (1983) *FEBS Lett. 154*, 328–334.
Rutherford, A. W., & Zimmerman, J. L. (1984) *Biochim. Biophys. Acta 767*, 168–175.
Rutherford, A. W., Zimmerman, J. L., & Mathis, P. (1984) in *Advances in Photosynthesis Research* (Symbesma, C., Ed.) Vol. 1, pp 445–448, Martinus Nijhoff/Dr. W. Junk Publishers, The Netherlands.
Sinning, I., Michel, H., Mathis, P., & Rutherford, A. W. (1989a) *FEBS Lett. 256*, 192–194.
Sinning, I., Michel, H., Mathis, P., & Rutherford, A. W. (1989b) *Biochemistry 28*, 5544–5553.
Vermaas, W. F. J., & Rutherford, A. W. (1984) *FEBS Lett. 175*, 243–248.
Wraight, C. A. (1978) *FEBS Lett. 93*, 283–288.

Myosin Subfragment 1 and Structural Elements of G-Actin: Effects of S-1(A2) on Sequences 39–52 and 61–69 in Subdomain 2 of G-Actin†

Theresa Chen,* Missak Haigentz, Jr., and Emil Reisler
Department of Chemistry and Biochemistry and Molecular Biology Institute, University of California, Los Angeles, California 90024

Received October 25, 1991; Revised Manuscript Received December 31, 1991

ABSTRACT: The effect of myosin on the structure of two sequences on G-actin, a loop between residues 39 and 52 and a segment between residues 61 and 69 from the NH_2-terminus, was probed by limited proteolytic digestions of G-actin in the presence of the myosin subfragment 1 isozyme S-1(A2). Under the experimental conditions of this work, no polymerization of actin was induced by S-1(A2) [Chen & Reisler (1991) *Biochemistry 30*, 4546–4552]. S-1(A2) did not change the rates of subtilisin and chymotryptic digestion of G-actin at loop 39–52. In contrast to this, the second protease-sensitive region on G-actin, segment 61–69, was protected strongly by S-1(A2) from tryptic cleavage. The minor if any involvement of loop 39–52 in S-1 binding was confirmed by determining the binding constants of S-1(A2) for pyrene-labeled G-actin (1.2×10^6 M^{-1}), subtilisin-cleaved pyrenyl G-actin (0.3×10^6 M^{-1}), and DNase I–pyrenyl G-actin complexes (0.3×10^6 M^{-1}). Consistent with this, the activity of DNase I, which binds to actin loop 39–52 [Kabsch et al. (1990) *Nature 347*, 37–44], was inhibited almost equally well by actin in the presence and absence of S-1(A2). These results confirm the observation that DNase I and S-1(A2) bind to distinct sites on actin [Bettache et al. (1990) *Biochemistry 29*, 9085–9091] and demonstrate myosin-induced changes in segment 61–69 of G-actin.

An intriguing feature of actin is its ability to interact with a large and ever-increasing number of proteins. In muscles, actin is organized into thin filaments within the myofibrils. The adenosine 5′-triphosphate (ATP)[1]-dependent interaction between filaments of actin and myosin is the basis of muscle contraction and any actomyosin-based cell motility. In non-muscle cells, actin is present in polymerized and depolymerized forms, and the equilibrium between these states is regulated

† This work was supported by Grant AR 22031 from the National Institutes of Health and by Grant DMB 89-05363 from the National Science Foundation.

[1] Abbreviations: ATP, adenosine 5′-triphosphate; DTT, dithiothreitol; FITC, fluorescein 5-isothiocyanate; MBS, *O*-(*m*-maleimidobenzoyl)-*N*-hydroxysuccinimide ester; PFPITC, pentafluorophenyl isothiocyanate; PMSF, phenylmethanesulfonyl fluoride; pyrenyl actin, actin modified at Cys-374 with *N*-(1-pyrenyl)iodoacetamide; S-1, myosin subfragment 1; S-1(A2), S-1 isozyme with alkaline light chain 2; SDS, sodium dodecyl sulfate.

0006-2960/92/0431-2941$03.00/0